PERGAMON

International Journal of Heat and Mass Transfer 45 (2002) 1643–1652

International Journal of HEAT and MASS TRANSFER

www.elsevier.com/locate/ijhmt

Constructal design for cooling a disc-shaped area by conduction

L.A.O. Rocha [a], S. Lorente [b], A. Bejan [a,*]

[a] *Department of Mechanical Engineering and Materials Science, School of Engineering, Duke University, Box 90300, Durham, NC 27708-0300, USA*

[b] *Department of Civil Engineering, National Institute of Applied Sciences (INSA), 135 Avenue de Rangueil, Toulouse 31077, France*

Received 14 May 2001; received in revised form 15 August 2001

Abstract

This paper describes a hierarchical strategy to developing the optimal internal structure of a round heat-generating body cooled at its center with the help of optimally distributed inserts of high-conductivity material. The sequence begins with optimizing the geometry of the smallest heat generating entity – a sector-shaped elemental volume with the smallest dimension, and a single high-conductivity insert. Many such elements are assembled into disc-shaped constructs, or into sector-shaped constructs in which the elemental volumes are grouped into a formation shaped as a fan. When several sector-shaped constructs are assembled into a disc, they constitute a quasi-radial heat-flow structure in which each high-conductivity insert exhibits one branching. Every geometric detail of the optimized two-material conductive structures is determined based on principle – the minimization of global resistance subject to global constraints (total volume, total volume of high-conductivity material). The inserts of high-conductivity material form structures shape as trees. The global thermal resistance of each tree-shaped construct is reported. The minimization of global thermal resistance is the criterion for choosing between a design with radial inserts and one with branched inserts.

Keywords: Constructal design; Electronics cooling; Tree networks; Topology optimization; Conduction

1. Multiple scales, increasing complexity, construction

The world of science and technology is racing toward smaller scales. The present paper is about a class of research opportunities that can be found in this direction. These go hand in hand with the interest in phenomena and devices at smaller scales. To illustrate, we use the problem of cooling with minimal thermal resistance a finite volume that generates heat at every point. This is a fundamental problem in the cooling of electronics [1–13]. The volume is much larger than the elemental building blocks – the 'atoms' of a structure that must be determined.

Our objective is to illustrate a generally applicable *hierarchical strategy* [1] for the design and optimization of complex macroscopic systems that employ smaller and smaller scales. The need for considering the broad picture – the macro system – is great and universal. No matter how successful we are in discovering and understanding small-scale phenomena and processes, we are forced to face the challenge of assembling these invisible elements into palpable devices. The challenge is to *construct*, i.e., to assemble and to optimize while assembling. This challenge is becoming more difficult, because while the smallest scales are becoming smaller, the complexity of the useful device (always macroscopic) becomes correspondingly greater.

This observation deserves emphasis, because it is widely overlooked in discussions of shrinking scales and nanotechnology. Technology means a lot more than the new physics that may appear on the frontiers of progressively smaller scales. A technology is truly new when

* Corresponding author. Tel.: +1-919-660-5309; fax: +1-919-660-8963.

E-mail address: dalford@duke.edu (A. Bejan).

0017-9310/02/$ - see front matter
PII: S0017-9310(01)00269-1

Nomenclature

A	area (m^2)
A_p	area of high-conductivity material (m^2)
$B_{1,2}$	dimensionless thermal resistance (Eqs. (14) and (42))
c	factor (Eq. (18))
D	thickness (m)
$\tilde{D}$	ratio of thicknesses (Eq. (37))
h	transversal dimension (m, Fig. 2)
H	periphery half-length (Fig. 2)
k_p	high-thermal conductivity (W/m K)
k_0	low-thermal conductivity (W/m K)
$\tilde{k}$	ratio of thermal conductivities (k_p/k_0)
n	number of peripheral elements (Fig. 3)
N	number of sectors (Fig. 1)
N	number of peripheral elements (Fig. 4)
q	heat current (W)
q'''	volumetric heat generation rate (W/m^3)
r	radial position (m)
R	radius (m)
$\tilde{R}$	dimensionless radius (Eq. (28))
R_s	thermal resistance (m K/W, Eq. (5))
$\tilde{R}_s$	dimensionless thermal resistance (Eq. (10))
t	thickness (m)
T	temperature (K)
T_c	corner temperature (K, Fig. 4)
T_0	center temperature (K, Fig. 1)

Greek symbols

α, β	angles (rad, Fig. 3)
ϕ	volume fraction of high-conductivity material

Subscripts

max	maximum
opt	optimum
R	peripheral position
s	sector
0	central position
1	position near the periphery

it is made useful in the form of devices (macroscopic constructs) that improve our lives. Usefulness demands that we must discover not only new physics, but also the strategy for packing and connecting the smallest-scale elements into devices for use at our macroscopic scales.

For example, if the smallest-scale element is the alveolus of the human lung, knowing only the biophysics of the alveolus is not enough. Worse still, the element alone does not reveal its purpose, or why a flow system of such a small scale must exist. We must also know how to assemble into our fixed volume (the thorax) the largest number of alveoli, and how to connect them (air ducts, blood vessels) such that the resulting macroscopic flow structure (the lung) achieves maximum performance under the constraints.

For this we need a strategy, or a principle of construction: assembly and optimization at every step, and at every scale. The physical structure that emerges at the macroscopic level is the result of following a strategy (principle) at every step of assembly or complexity increase. Likewise, in the human lung the many trees for air flow and blood flow are the results of principle: the relentless pursuit of smaller and smaller flow resistances when space is at a premium.

Our strategy is to start from the smallest scale, e.g., the elemental volume optimized in Section 3. The first challenge is to understand the functioning of elemental systems, and to optimize their performance subject to their own, smallest-scale space constraints. Next is the challenge to assemble and optimize the relative positions of a number of elements systems into a larger and fixed space. The resulting flow system is a first construct [1]. This procedure can be continued toward stepwise larger scales, in steps of aggregation combined with optimization under global constraints.

Just as in the human lung, the structure of the macroscopic system will be a *complex* one, with many tree-shaped paths for the flowing currents, and with elemental systems filling the interstices – the spaces between the smallest branches of the flow trees. This structure will be characterized by *multiple scales* – entire arpeggios of length, time and force scales. This structure will be noted for its *geometry* – numbers of constituents in each construct relative positions, relative thicknesses of connecting ducts, and angles of confluence. All these commonly observed features, complexity, multiple scales, and architecture in three-dimensions, are results of the consistent reliance on strategy. They are not haphazard.

To think about small-scales technology in these terms is to make a step forward in the philosophy of engineering design. This step is particularly timely in view of the computational tools that are available today. Traditional design begins with assuming one configuration, building a model (a facsimile of the configuration), and optimizing its performance. If time and money permit, one or two alternative configurations are modeled and optimized, so that in the end the designer may select the best configuration from the assumed few.

As an alternative, the 'constructal' strategy illustrated in this paper liberates the designer from the straight jacket represented by *modeling* (the assumption of a certain macroscopic structure). Our view is that the physical configuration is the chief unknown in design, and that the optimization of configuration (morphol-

ogy) is the route to maximum global system performance. Painfully unknown at the start is the configuration of the complex flow system that will eventually fit inside the specified (constrained) macroscopic volume. The illustrated construction and optimization proceed freely, that is, with architecture as a set of geometrical variables that can be optimized at each level of assembly. Geometry is not random – it results from principle, which is why the tree architecture is everywhere, in nature and engineering [1]. Geometry makes systems achieve their best. Geometry matters.

2. Volume-to-point heat flow

Consider the problem of cooling with one central heat sink (T_0), a disc-shaped body with uniform distribution of heat generation rate, Fig. 1. In this two-dimensional geometry the heat generation rates per unit volume and unit area are, respectively, q''' and $q'''t$, where t is the thickness of the disc in the direction perpendicular to the plane of Fig. 1. The thermal conductivity of the body is k_0. The body temperature is above T_0 such that the generated heat current flows into the center. We seek ways to minimize the global thermal resistance, i.e., the hot spot temperature T_{max}, which is likely to occur on the rim.

One way to decrease the global resistance is to insert through the k_0 medium an amount of material with considerably higher thermal conductivity, k_p. The composition of the two-material composite is fixed, and is accounted for by the volume fraction

$$\phi = (\text{volume of } k_p \text{ material})/(\text{total volume}). \quad (1)$$

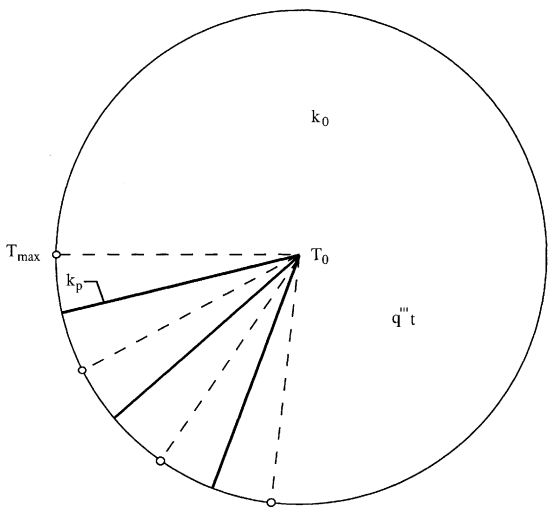

Fig. 1. Disc-shaped body with uniform heat generation, central heat sink, and radial pattern of high-conductivity paths.

The challenge that comes with designing the composite is to optimize the geometry of the paths for heat transfer. The question is how to distribute the k_p-paths on the k_0 background, how to shape the k_0 material that is allocated to one blade of k_p material, and how to connect k_p-blades to each other and to the central heat sink. This problem was considered for systems shaped as rectangles [14], where the hierarchical constructal method was formulated. In this paper we extend the method to the cooling of a round volume, because disc-shaped assemblies are often encountered in the packaging of electronics [15].

The simplest architectural feature that can be anticipated intuitively is that the thin blades of k_p material (the 'nerves' of the heat flow structure) must be arranged radially and equidistantly with one end touching the heat sink. In the simplest design, the k_p blades do not have branches and stretch radially all the way to the rim. As shown in Fig. 1, to each k_p blade corresponds a circular sector with adiabatic radial sides (dashed lines). More complex constructs with branches form the subject of Sections 5 and 6.

3. Elemental volume

The most fundamental feature of constructal designs for volume-point and area-point paths is that the smallest volume (or area) scale of the flow structure is known and fixed. The smallest scale is invariant, i.e., independent of the system into which the more and more complex flow structure may grow. In applications such as the cooling of small-scale electronics, the smallest volume scale is often dictated by manufacturing constraints, electromagnetic interference between neighboring components, and the space competition between electrical and thermal design functions.

The elemental volume of the flow structures constructed in this work is the sector of circle isolated in Fig. 2. We assume that there are many radial k_p blades so that one sector is sufficiently slender to be approximated by an isosceles triangle of base $2H$ and height R. The area of the elemental sector is fixed,

$$A_s = HR \quad (2)$$

in accordance with the constraints reviewed in the preceding paragraph. The dimensions H and R may vary. The chief unknown of the architecture is the shape of the sector: the aspect ratio of the element, H/R, or the tip angle of the circular sector, or the number of elements (or blades) that should be assembled into a complete disc (Fig. 1).

The second constraint of the elemental architecture is the volume fraction of k_p material

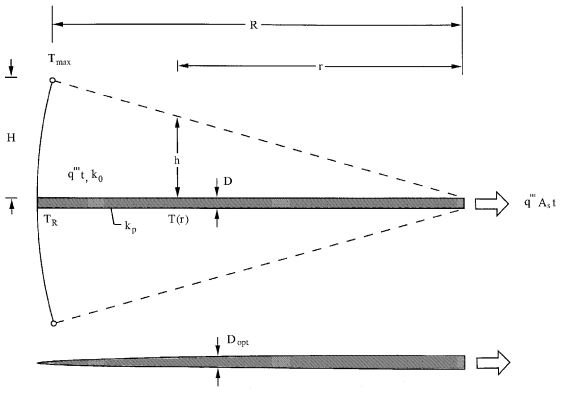

Fig. 2. Elemental system: circular sector with high-conductivity blade on its center line, and the optimal blade shape.

$$\phi = \frac{DR}{HR} = \frac{D}{H}, \tag{3}$$

where D is the thickness of the k_p blade. For the sake of simplicity in analysis, we assume that

(1) The thickness D is constant,
(2) The k_p volume fraction is fixed and small, $\phi \ll 1$, and
(3) The ratio of thermal conductivities is fixed and large,

$$\tilde{k} = \frac{k_p}{k_0} \gg 1. \tag{4}$$

It is shown later in Eq. (11) that assumption (3) is consistent with the slenderness assumption $H/R \ll 1$ when the design of the element is optimized for minimum overall thermal resistance. Assumption (1) is relaxed in Section 5. Assumption (2) means that the k_p blade is sufficiently thin to be represented by the axis of symmetry in Fig. 2 (the $T_R - T_0$ line).

The objective in optimizing the geometry of the elemental sector is to minimize the global thermal resistance of the sector,

$$R_s = \frac{T_{max} - T_0}{q''' A_s}, \tag{5}$$

where $q''' A_s$ is the heat current generated over the entire sector. We evaluate this in a two-part analysis, by calculating $(T_{max} - T_R)$ and $(T_R - T_0)$. This decoupling is possible because under assumptions (2) and (3) the thermal diffusion through the k_0 material is perpendicular to the k_p blade, and the conduction through the k_p material is oriented radially, along the blade.

In the analysis of vertical k_0 conduction along the line $T_{max} - T_R$, we note that there is heat generation at every point, the T_{max} end is insulated, and the T_R end (the contact with the k_p blade) is the heat sink. This means that the temperature distribution is parabolic between the points T_R and T_{max}, and has zero slope at T_{max}. Because of the parabolic distribution, the vertical temperature gradient felt at the T_R point is $2(T_{max} - T_R)/H$. We account for the conservation of energy in the string-shaped fiber $T_R - T_{max}$ by equating the heat current generated in the fiber $(q''''H)$ with the heat flux leaving the fiber through the T_R end, namely, $q'''H = k_0 2(T_{max} - T_R)/H$. From this we deduce the temperature difference between the hot spot and the tip of the high-conductivity blade:

$$T_{max} - T_R = \frac{q'''H^2}{2k_0}. \tag{6}$$

In the analysis of conduction along the k_p blade, we note that the heat current that flows toward the center increases from $q = 0$ at $r = R$ to the total current $q = q'''tA$ at $r = 0$. The increase experienced by q at an intermediate position (r) is

$$-\mathrm{d}q = 2hq'''t\,\mathrm{d}r, \tag{7}$$

where $hq'''t$ is the heating collected over the vertical surface ht, where $h = (H/R)r$. The heat current is proportional to the local temperature gradient:

$$q = k_p Dt \frac{\mathrm{d}T}{\mathrm{d}r}. \tag{8}$$

We determine $(T_{max} - T_R)$ by eliminating q between Eqs. (7) and (8), integrating twice in r, and invoking the boundary conditions $\mathrm{d}T/\mathrm{d}r = 0$ at $r = R$, and $T = T_0$ at $r = 0$:

$$T_R - T_0 = \frac{2q'''R^2}{3k_p\phi}. \tag{9}$$

The global resistance of the elemental sector is obtained by adding Eqs. (6) and (9), and nondimensionalizing R_s by using the background conductivity k_0,

$$\tilde{R}_s = \frac{T_{max} - T_0}{q''' A_s/k_0} = \frac{1}{2}\frac{H}{R} + \frac{2}{3\tilde{k}\phi}\frac{R}{H}. \tag{10}$$

This expression can be minimized with respect to the aspect ratio of the element, H/R, and the results are

$$\left(\frac{H}{R}\right)_{opt} = \frac{2}{(3\tilde{k}\phi)^{1/2}} \ll 1, \tag{11}$$

$$\frac{(T_{max} - T_0)_{min}}{q''' A_s/k_0} = \frac{2}{(3\tilde{k}\phi)^{1/2}}. \tag{12}$$

Eq. (11) shows that the assumed slenderness of the optimized sector is consistent with assumption (3): the ratio of conductivities $\tilde{k}$ must exceed $1/\phi$ in an order of magnitude sense.

4. Disc-shaped assembly or the first construct

The aspect ratio (11) fixes the tip angle of the sector. It also fixes the number of such sectors that fit in a complete disc arrangement, $N = 2\pi R/(2H)$, namely

$$N = \frac{\pi}{2}(3\tilde{k}\phi)^{1/2} \gg 1. \tag{13}$$

The corresponding thermal resistance of the entire disc is obtained by using NA_s instead of A_s in Eq. (12)

$$B_1 = \frac{(T_{max} - T_0)}{q'''NA_s/k_0} = \frac{4}{3\pi\tilde{k}\phi}. \tag{14}$$

The radius of the disc-shaped construct is

$$R = (A_s/2)^{1/2}(3\tilde{k}\phi)^{1/4}. \tag{15}$$

The size of the construct (R) is not known a priori. It is the result of optimization, assembly and the constraints that govern the smallest-scale element ($A_s, \phi, \tilde{k}$). Aggregation, organization, growth and complexity are the result of geometric constraints – trying to fit together a number of smaller optimized parts. A key role is played by the product $\tilde{k}\phi$: larger values mean more high-conductivity blades, more slender blades, and a disc-shaped construct with larger radius R. We reexamine these properties in the discussion of Fig. 9.

5. Optimally shaped inserts

Further improvements in the performance of the construct can be made by relaxing some of the simplifying assumptions, increasing the number of degrees of freedom of the design, and optimizing the design with respect to the new degrees of freedom [1]. One example is the constant-D assumption (1) on which the results of Section 4 are based. Consider instead the general function $D(r)$ that is subjected to the same volume fraction constraint,

$$\phi = \frac{1}{HR}\int_0^R D\,\mathrm{d}r. \tag{16}$$

The choice of k_p-blade profile $D(r)$ affects the global resistance through the part $T_R - T_0$. This relationship is obtained by eliminating q between Eqs. (7) and (8), integrating the resulting equation once in r, invoking $\mathrm{d}T/\mathrm{d}r = 0$ at $r = R$, and finally integrating from $r = 0$ to $r = R$:

$$T_R - T_0 = \frac{q'''H}{k_p R}\int_0^R \frac{R^2 - r^2}{D}\,\mathrm{d}r. \tag{17}$$

Variational calculus delivers the function $D(r)$ that minimizes integral (17) subject to constraint (16)

$$D_{opt} = c(R^2 - r^2)^{1/2}. \tag{18}$$

The factor c is calculated by substituting Eq. (18) into constraint (16)

$$D_{opt} = \frac{4}{\pi}\phi H\left[1 - \left(\frac{r}{R}\right)^2\right]^{1/2}. \tag{19}$$

The optimal shape of the high-conductivity blade is such that the root is thicker and the tip is blunt ($\mathrm{d}D/\mathrm{d}r = -\infty$ at $r = R$), as shown in the lower part of Fig. 2. These characteristics match those of other optimized shapes of elemental inserts, nerves and needles [1]. They also agree with the features of natural dendrites.

The analytical steps of Section 4 can be repeated with $D_{opt}(r)$ in place of $D =$ constant. Eqs. (11)–(15) are replaced, in order, by

$$\left(\frac{H}{R}\right)_{opt} = \frac{\pi/2}{(2\tilde{k}\phi)^{1/2}}, \tag{20}$$

$$\frac{(T_{max} - T_0)}{q'''A_s/k_0} = \frac{\pi/2}{(2\tilde{k}\phi)^{1/2}}, \tag{21}$$

$$N = 2(2\tilde{k}\phi)^{1/2} \gg 1, \tag{22}$$

$$\frac{(T_{max} - T_0)_{min}}{q'''NA_s/k_0} = \frac{\pi}{8\tilde{k}\phi}, \tag{23}$$

$$R = (2A_s/\pi)^{1/2}(2\tilde{k}\phi)^{1/4}. \tag{24}$$

The decrease in the thermal resistance of the sector is evaluated by dividing Eq. (21) by Eq. (12): the result is $(\pi/4)(3/2)^{1/2} = 0.96$, or a 4% decrease. The resistance decrease registered by the entire disc assembly is estimated by dividing Eq. (23) by Eq. (14): the result is $3\pi^2/32 = 0.925$, which indicates a 7.5 reduction in global resistance.

6. One level of branching, or the second construct

Natural and engineered flow structures exhibit an additional feature: they become more complex and more efficient as they fill larger spaces. In this section we seek to determine whether this is also true in the case of a network of high-conductivity blades that cools a disc-shaped system with uniform heat generation. We begin with a structure with just one level of complexity above that of the radial pattern of Fig. 1: one k_p blades stretches radially to the distance L_0 away from the central heat sink, and continues with a number (n) of branches (or, better, tributaries) that reach the rim. In place of the elemental sector of Fig. 2, we now analyze the sector with one stem (L_0, D_0) and n tributaries (L_1, D_1) shown in Fig. 3. The goal is to assemble with minimum flow resistance a number (N) of branched sectors into a complete disc, as shown in Fig. 4.

The following analysis is based on the main result of Section 3: one isolated sector with a single central blade

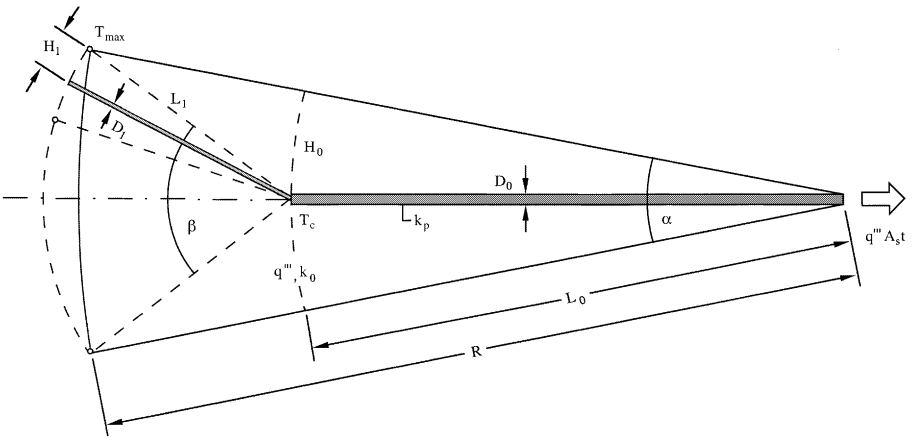

Fig. 3. One level of branching: one central high-conductivity path (L_0, D_0) with n_1 smaller paths (L_1, D_1) as tributaries.

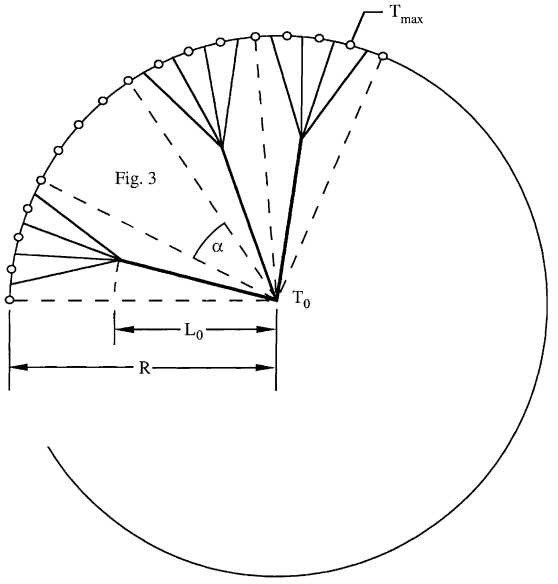

Fig. 4. Disc-shaped body cooled by a structure consisting of several of the branched sectors shown in Fig. 3.

has an optimal aspect ratio when its size and amount of k_p material are fixed, and when its global resistance to heat transfer must be minimized. To use this property, in Fig. 3 we view the construct as a combination of n small sectors of aspect ratio H_1/L_1, plus a central sector of aspect ratio H_0/L_0. The length L_1 is the distance from the hot spot (T_{max}) to the point of confluence (T_c).

The number of tributaries (n) is an important feature on which the complexity and manufacturability of the structure rests. This feature is particularly important in view of earlier results that show pairing ($n_1 = 2$) as the best option when the constructs have rectangular shapes [1,14]. Is pairing or bifurcation always recommended?

We assume that each peripheral sector of radius L_1 is slender enough such that the optimized shape of Eq. (11) is correct:

$$\frac{H_1}{L_1} = \frac{2}{(3\tilde{k}\phi_1)^{1/2}}, \quad \phi_1 = \frac{D_1}{H_1}, \quad A_1 = H_1 L_1. \tag{25}$$

The same cannot be said about the central sector of radius L_0, because, unlike in Section 3, the T_c end of its high-conductivity blade is not insulated. For this reason the aspect ratio of the (H_0, L_0) sector is free to vary, and so is the aspect ratio of the entire sector (radius R) of Fig. 3. For the (H_0, L_0) sector we write only

$$\frac{H_0}{L_0} \cong \frac{\alpha}{2}, \quad A_0 = H_0 L_0, \tag{26}$$

where the tip angle α is a function of the assumed n and R values. The number of A_1 elements that fit along the perimeter of the R disc is $N = 2\pi R/(2H_1)$. The number of branched sectors of angle α is N/n. The angle α is then

$$\alpha = \frac{2\pi n}{N} = \frac{2^{3/2} n}{R(3\tilde{k}\phi_1)^{1/4}}, \tag{27}$$

where the dimensionless radius $\tilde{R}$ is based on $A_1^{1/2}$ as the specified (fixed) elemental length scale of the structure,

$$\tilde{R} = \frac{R}{A_1^{1/2}}. \tag{28}$$

The area A_0 that is allocated to the stem (L_0, D_0) is $(\alpha/2)L_0^2$, where $L_0 \cong R - L_1$. After some algebra, we obtain

$$A_0 \cong \frac{2^{1/2} n \tilde{R} A_1}{(3\tilde{k}\phi_1)^{1/4}} \left[1 - \frac{(3\tilde{k}\phi_1)^{1/4}}{2^{1/2}\tilde{R}}\right]^2. \tag{29}$$

Note that Eq. (29) is approximate because not all the A_1 elements have the length L_1. This approximation becomes more accurate as the angles β and α decrease.

Next, we estimate the overall thermal resistance $(T_{\max} - T_0)/(q'''A)$. We do this in two parts. For the overall temperature difference sustained by the corner sector of radius L_1 we deduce from Eq. (12) that

$$T_{\max} - T_c = \frac{2q'''A_1}{k_0(3\tilde{k}\phi_1)^{1/2}}. \tag{30}$$

The temperature drop from the junction (T_c) to the central link (T_0) requires a new analysis, because unlike Eqs. (7)–(9) the T_c tip of the D_0 blade receives the heat current collected by the n peripheral sectors of size A_1,

$$q'''tnA_1 = k_p D_0 t\left(\frac{dT}{dt}\right)_{r=L_0}. \tag{31}$$

As in Fig. 2, the radial position in central sector of Fig. 3 is measured from the center ($r = 0$) to the T_c junction ($r = L_0$). The temperature distribution along the D_0 blade is obtained by starting with the equivalent of Eqs. (7) and (8),

$$-dq = 2\left(\frac{H_0}{L_0}r\right)q'''t\,dr, \tag{32}$$

$$q = k_p D_0 t\frac{dT}{dr} \tag{33}$$

eliminating q, integrating twice in r, and invoking the tip condition (31) and $T = T_0$ at $r = 0$. In the resulting $T(r)$ expression we set $T(L_0) = T_c$, and obtain

$$T_c - T_0 = \frac{q'''L_0}{k_p D_0}\left(\frac{2}{3}A_0 + nA_1\right). \tag{34}$$

Adding Eqs. (30) and (34), and noting again that $L_0 \cong R - L_1$, we obtain the temperature difference

$$T_{\max} - T_0 \cong \frac{2q'''A_1}{k_0(3\tilde{k}\phi_1)^{1/2}} + \frac{q'''(R-L_1)}{k_p D_0}\left(\frac{2}{3}A_0 + nA_1\right). \tag{35}$$

This quantity can be nondimensionalized as

$$\tilde{T} = \frac{T_{\max} - T_0}{q'''A_1/k_0} = \frac{2}{\left(3\tilde{k}\phi_1\right)^{1/2}} + \frac{\left(3\tilde{k}\phi_1\right)^{1/4}}{2^{1/2}\tilde{k}\phi_1\tilde{D}}\left[\tilde{R} - \frac{\left(3\tilde{k}\phi_1\right)^{1/4}}{2^{1/2}}\right] \times \left\{\frac{2^{3/2}n\tilde{R}}{3\left(3\tilde{k}\phi_1\right)^{1/4}}\left[1 - \frac{\left(3\tilde{k}\phi_1\right)^{1/4}}{2^{1/2}\tilde{R}}\right]^2 + n\right\}, \tag{36}$$

where $\tilde{D}$ is the ratio of k_p-blade thicknesses:

$$\tilde{D} = \frac{D_0}{D_1}. \tag{37}$$

The temperature difference $\tilde{T}$ depends on geometry $(n, \tilde{D}, \tilde{R})$, and on the presence of k_p material $(\tilde{k}, \phi_1)$. The total amount of k_p material in the R disc is represented by the cross-sectional area

$$A_p = ND_1L_1 + \frac{N}{n}D_0L_0 \tag{38}$$

or by the fraction that A_p occupies in the entire disc (πR^2):

$$\phi = \frac{A_p}{\pi R^2} = \frac{\left(3\tilde{k}\phi_1\right)^{1/4}\phi_1}{2^{1/2}\tilde{R}} + \frac{\tilde{D}\phi_1}{n\tilde{R}}\left[\tilde{R} - \frac{\left(3\tilde{k}\phi_1\right)^{1/4}}{2^{1/2}}\right]. \tag{39}$$

The ϕ fraction is fixed (e.g., $\phi = 0.1$), and provides a relation between $\tilde{k}$, ϕ_1, $\tilde{D}$, n and $\tilde{R}$. The $\tilde{k}$ ratio is fixed by the choice of materials (e.g., $\tilde{k} = 300$). We expect a tradeoff between ϕ_1 and $\tilde{D}$, which will represent the optimal allocation of k_p material to the D_0 and D_1 blades.

To start with, we set $n = 2$ and $\tilde{R} = 4$, and minimized $\tilde{T}$ by varying ϕ_1 and $\tilde{D}$, where ϕ_1 and $\tilde{D}$ are related by Eq. (39). Fig. 5 confirms that $\tilde{T}$ has a minimum with respect to how the k_p-material is allocated. The resulting features of the optimal configuration ($\phi_{1,\text{opt}}$, $\tilde{D}_{\text{opt}}$, $\tilde{T}_{\min}$) are reported in Fig. 6. This figure also shows how the optimum responds to changes in the size of the construct, $\tilde{R}$. The optimal allocation of high-conductivity material is almost insensitive to changes in $\tilde{R}$. The temperature difference $\tilde{T}_{\min}$ is almost proportional to $\tilde{R}$.

The numerical work summarized in Fig. 6 was repeated for other numbers of elemental branches, $n = 4, 6, \ldots$ The key feature of these results is that the $\phi_{1,\text{opt}}$ and $\tilde{T}_{\min}$ curves, which in Fig. 6 were plotted for $n = 2$, do not shift as n increases. Fig. 7 shows that the $\tilde{D}_{\text{opt}}$ curve rises as n increases. A larger $\tilde{D}_{\text{opt}}$ means an elemental insert (D_1) that is thinner relative to the stem (D_0). The numerical values plotted in Fig. 7 indicate that $\tilde{D}_{\text{opt}}/n$ is almost constant, which means that the optimum is characterized by $D_0 \approx nD_1$. This approximation is more exact when $\tilde{R}$ is smaller. In this limit, the cross-sectional area of the k_p-inserts is conserved at the junction between the stem and the branches. When $\tilde{R}$ is larger, the stem cross-section is larger than the combined cross-section of the branches, $D_0 > nD_1$.

Fig. 6 also shows the required total number of peripheral elements:

$$N_{\text{opt}} = 2^{-1/2}\pi\tilde{R}(3\tilde{k}\phi_{1,\text{opt}})^{1/4}. \tag{40}$$

This number increases as $\tilde{R}$ increases, and is independent of n. The corresponding central length scale of the optimized branched pattern, $\tilde{L}_{\text{opt}} = L_{0,\text{opt}}/A_1^{1/2}$, is obtained by writing $L_0 = R - L_1$ and using the first of Eq. (25):

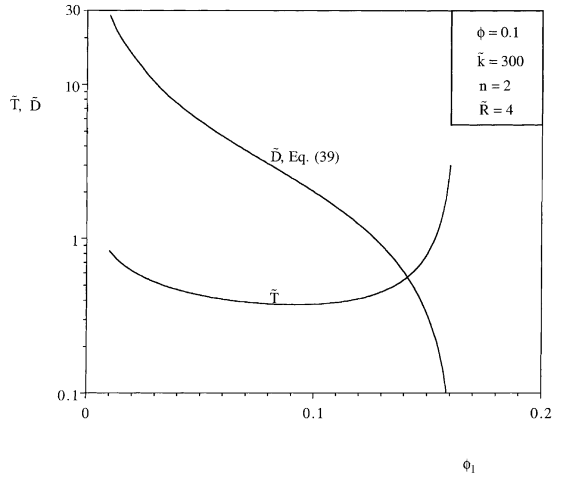

Fig. 5. The minimization of the overall temperature difference in the disc-shaped construct of Fig. 4.

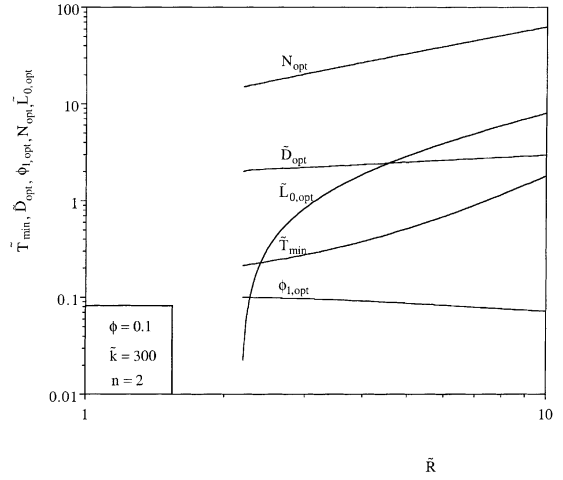

Fig. 6. The effect of the disc size ($\tilde{R}$) on the optimal configuration determined in Fig. 5.

$$\tilde{L}_{\text{opt}} = \tilde{R} - 2^{-1/2}(3\tilde{k}\phi_{1,\text{opt}})^{1/4}. \tag{41}$$

This length increases with $\tilde{R}$, and is independent of n (Fig. 6). Note that L_0 shrinks to zero (hence $\phi_{1,\text{opt}} = \phi$) when $\tilde{R}$ drops to 2.18: this critical $\tilde{R}$ value corresponds to the optimized radial pattern without branches (Fig. 1), as we will see again in Fig. 8. The disappearance of the branched pattern at $\tilde{R} = 2.18$ is the reason why all the curves in Fig. 6 vanish below $\tilde{R} = 2.18$.

7. Growth and complexity: mechanisms for decreasing the global resistance

In each of the cases optimized in Figs. 5–7 the elemental area A_1 and the disc size R were fixed. This means

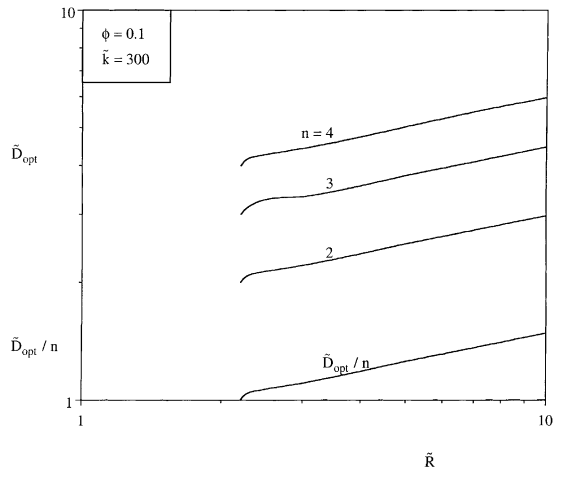

Fig. 7. The effect of the number of elemental branches (n) on the optimized ratio of the k_p-insert thicknesses ($\tilde{D}_{\text{opt}}$).

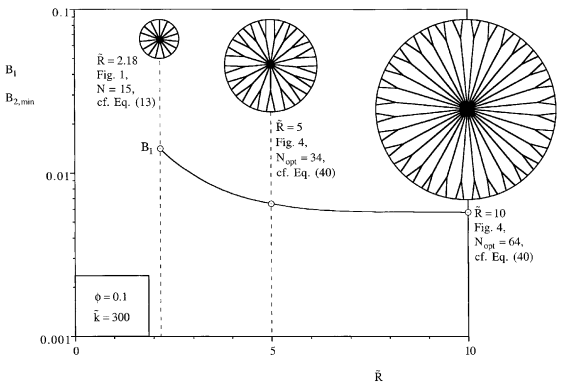

Fig. 8. The overall thermal resistances of the optimized radial pattern (B_1) and the optimized branched patterns ($B_{2,\text{min}}$).

that the minimization of $\tilde{T}$ is equivalent to the minimization of the overall thermal resistance of the entire disc,

$$B_2 = \frac{T_{\max} - T_0}{q'''\pi R^2/k_0} = \frac{\tilde{T}}{\pi\tilde{R}^2}. \tag{42}$$

Because $\tilde{T}_{\min}$ is almost proportional to $\tilde{R}$, the minimized resistance $[B_{2,\min} = \tilde{T}_{\min}/(\pi\tilde{R}^2)]$ decreases almost as $\tilde{R}^{-1}$ as $\tilde{R}$ increases. Growth, or system expansion emerges as a route to the optimization of access for the heat currents that must be collected on and evacuated from the disc.

The minimized resistance $B_{2,\min}$ depends on $\tilde{R}$, $\tilde{k}$ and ϕ. It does not depend on n because $\tilde{T}_{\min}$ does not depend on n. If we compare this resistance ($B_{2,\min}$) with the corresponding resistance (B_1) of the disc with radial inserts (Fig. 1), we can determine the recommended 'transition' from radial patterns to branched patterns. We make this comparison based on the same elemental

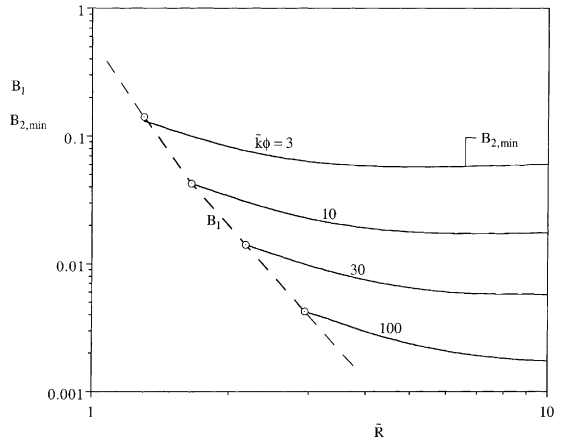

Fig. 9. The effect of $\tilde{k}$ and ϕ on the overall thermal resistances of the optimized radial and branched patterns.

size ($A_s = A_1$) and the same amounts and properties of conducting materials ($\tilde{k}$, ϕ). The dimensionless radius of the radial design of Section 4 is, cf. Eq. (15),

$$\tilde{R} = 2^{-1/2}(3\tilde{k}\phi)^{1/4}. \quad (43)$$

In Fig. 1, this radius is fixed when $\tilde{k}$ and ϕ are fixed. In the branched design $\tilde{R}$ can be increased freely. This is why in Fig. 8 one case ($\tilde{k}$, ϕ) is represented by one radial-design point $B_1(\tilde{R})$ and one branched-design curve $B_{2,\min}(\tilde{R})$. The figure shows that when $\tilde{R}$ exceeds 2.18 (in the case $\phi = 0.1$, $\tilde{k} = 300$), the global resistance is smaller when the high-conductivity material is distributed according to the optimized branched pattern. Once again, the global resistance can be decreased by enlarging the system and making it more complex (with branching).

We repeated the calculations of Fig. 8 for other values of $\tilde{k}$ and ϕ, in the range $30 \leqslant \tilde{k} \leqslant 1000$ and $0.01 \leqslant \phi \leqslant 0.1$. We found the same qualitative behavior as in Fig. 8, and the additional feature that the effect of $\tilde{k}$ and ϕ on $B_{2,\min}$ is exercised through the product $\tilde{k}\phi$. Fig. 9 is a condensation of all these results. Lower global resistances are achieved by decreasing $\tilde{k}\phi$, and by switching from the optimized radial pattern (Fig. 1) to the optimized branched pattern (Fig. 4) when $\tilde{R}$ can be made greater than the $\tilde{R}$ value of the optimized radial pattern. Fig. 8 illustrates this transition in the case of $\tilde{k} = 300$ and $\phi = 0.1$, for which the radial pattern has $\tilde{R} = 2.18$ and 15 elemental sectors, and the branched pattern has 34 peripheral elements for $\tilde{R} = 5$ and 64 peripheral elements for $\tilde{R} = 10$.

8. Concluding remarks

In this paper we illustrated a hierarchical strategy for developing the optimal flow structure for cooling with high-conductivity inserts a disc-shaped body that generates heat at every point. The strategy consists of optimization of performance (resistance minimization) at every scale, followed by the assembly of optimized systems into larger systems. Every geometric detail of the heat flow structure is derived from principle. The flow structure is the construction (configuration) of the two-material conductive body.

The analytical work was simple enough to allow the construction to proceed to two levels of assembly, i.e., disc-shaped flow structures with one level of branching (Fig. 4). Beyond this stage, en route to cooling larger and larger heat-generating bodies, the method calls for optimizing structures with two levels of branching. This step would begin with optimizing the architecture of a sector-shaped construct such as Fig. 3, in which each of the sectors that make up the 'fan' of angle β has the one-branching structure optimized in this paper based on Fig. 3. Earlier work on the development of growing tree-shaped conductive trees in rectangular coordinates [1] suggests that, when plotted on Fig. 8, the global resistance curve of the two-branching structure would intersect the existing $B_{2,\min}(\tilde{R})$ curve for one-branching designs. This means that there is a second transition, at a higher $\tilde{R}$ value, where the choice of optimized patterns switches from one-branching designs to two-branching designs. The first transition, or the 'onset' of the first branching occurred at $\tilde{R} = 2.18$ for $\phi = 0.1$ and $\tilde{k} = 300$. There is an analogy between this pattern of successive transitions and the discrete transitions toward more complex flows in Bénard convection and turbulence, which is why the occurrence of the latter has also be reasoned on the basis of the construction strategy illustrated in this paper [1,16].

Acknowledgements

The work reported in this paper was supported by the National Science Foundation, and CAPES – Brasília, Brazil.

References

[1] A. Bejan, Shape and Structure, from Engineering to Nature, Cambridge University Press, Cambridge, UK, 2000.
[2] S.J. Kim, S.W. Lee, Air Cooling Technology for Electronic Equipment, CRC Press, Boca Raton, FL, 1995.
[3] G.P. Peterson, A. Ortega, Thermal control of electronic equipment and devices, Adv. Heat Transfer 20 (1990) 181–314.
[4] W. Aung (Ed.), Cooling Technology for Electronic Equipment, Hemisphere, New York, 1988.
[5] W. Li, S. Kakac, F.F. Hatay, R. Oskay, Experimental study of unsteady forced convection in a duct with and

without arrays of block-like electronic components, Wärme-und Stoffübertragung 28 (1993) 69–79.
[6] S.H. Kim, N.K. Anand, Laminar developing flow and heat transfer between a series of parallel plates with surface mounted discrete heat sources, Int. J. Heat Mass Transfer 37 (1994) 2231–2244.
[7] G. Guglielmini, E. Nanei, G. Tanda, Natural convection and radiation heat transfer from staggered vertical fins, Int. J. Heat Mass Transfer 30 (1987) 1941–1948.
[8] A. Bejan, E. Sciubba, The optimal spacing of parallel plates cooled by forced convection, Int. J. Heat Mass Transfer 35 (1992) 3259–3264.
[9] S. Petrescu, Comments on the optimal spacing of parallel plates cooled by forced convection, Int. J. Heat Mass Transfer 37 (1994) 1283.
[10] A. Bar-Cohen, W.M. Rohsenow, Thermally optimum spacing of vertical, natural convection cooled, parallel plates, J. Heat Transfer 106 (1984) 116–123.
[11] N.K. Anand, S.H. Kim, L.S. Fletcher, The effect of plate spacing on free convection between heated parallel plates, J. Heat Transfer 114 (1992) 515–518.
[12] S. Kakac, H. Yüncü, K. Hijikata (Eds.), Cooling of Electronic Systems, Kluwer Academic Publishers, Dordrecht, The Netherlands, 1994.
[13] R.W. Knight, J.S. Goodling, D.J. Hall, Optimal thermal design of forced convection heat sinks – analytical, J. Electron. Packaging 113 (1991) 313–321.
[14] A. Bejan, Constructal-theory network of conducting paths for cooling a heat generating volume, Int. J. Heat Mass Transfer 40 (1997) 799–816.
[15] D.V. Pence, Improved thermal efficiency and temperature uniformity using fractal-like branching channel networks, in: G.P Celata, V.P Carey, M. Groll, I. Tanasawa, G. Zummo (Eds.), Heat Transfer and Transport Phenomena, Begell House, New York, 2000, pp. 142–148.
[16] R.A. Nelson Jr., A. Bejan, Constructal optimization of internal flow geometry in convection, J. Heat Transfer 120 (1998) 357–364.